European Journal of Mechanics A/Solids 30 (2011) 54–62

Contents lists available at ScienceDirect

European Journal of Mechanics A/Solids

journal homepage: www.elsevier.com/locate/ejmsol

The characteristics of plastic flow and a physically-based model for 3003 Al–Mn alloy upon a wide range of strain rates and temperatures

W.G. Guo [a,*], X.Q. Zhang [a], J. Su [a], Y. Su [b], Z.Y. Zeng [c], X.J. Shao [c]

[a] School of Aeronautics, Northwestern Polytechnical University, Xi'an 710072, China
[b] School of Aerospace Engineering, Beijing Institute of Technology, Beijing 100081, China
[c] No.202 Institute of China Ordnance Industry, Xianyang 710099, China

ARTICLE INFO

Article history:
Received 31 December 2009
Accepted 1 September 2010
Available online 16 September 2010

Keywords:
Aluminum alloy
Constitutive model
Dynamic strain aging
Hopkinson bar
Plastic flow

ABSTRACT

The uniaxial compressive responses of 3003 Al–Mn alloy upon strain rates ranging from 0.001/s to about 10^4/s with initial temperatures from 77 K to 800 K were investigated. Instron servohydraulic testing machine and enhanced split Hopkinson bar facilities have been employed in such uniaxial compressive loading tests. The maximum true strain up to 80% has been achieved. The following observations have been obtained from the experimental results: 1) 3003 Al–Mn alloy presents remarkable ductility and plasticity at low temperatures and high strain rates; 2) its plastic flow stress strongly depends on the applied temperatures and strain rates; 3) the temperature history during deformation strongly affects the microstructure evolution within the material. Finally, paralleled with the systematic experimental investigations, a physically-based model was developed based on the mechanism of dislocation kinetics. The model predictions are compared with the experimental results, and a good agreement has been observed.

© 2010 Elsevier Masson SAS. All rights reserved.

1. Introduction

3003 Al–Mn alloy is considered an important engineering material in cryogenic systems and in aerospace applications (Woodcraft, 2005). Compared with other aluminum alloys, it presents very high strength and very good corrosion resistance (Luan et al., 2004). To widen the application field and improve the performance, the mechanical properties of 3003 Al–Mn alloy have been widely studied in past decades (Fujii et al., 2002; Liu et al., 2004; Yeh et al., 2003; Barlat et al., 2002). In many practical applications, however, 3003 Al–Mn alloy is subject to high rates of straining with different temperatures, such as during the course of high speed machining, impact energy absorbing, rapid crack propagating, metal forming, and other scenarios. Therefore the corresponding mechanical responses under different strain rates and temperatures need to be well understood. In this work, the results of a series of quasi-static (less than 0.1/s) and dynamic (3200 and 9500/s) compression tests on 3003 Al–Mn alloy are first investigated. These tests are performed over a temperature range from 77 K to 820 K. Based on the observation of experimental results, and by considering the evolution of the microstructure and the effects of long-range and short-range barriers to the motion of dislocations, the flow stress of 3003 Al–Mn alloy under different strain rates and temperatures is modeled using a developed physically-based model. The corresponding model predictions are then compared with the experimental observations.

2. Experimental procedures

All tests are carried out on 3003 Al–Mn alloy base plates, which are commercially available with the specific chemical composition given in Table 1. Both the nominal diameter and height of the samples are designed to be 5 mm. Ends of samples are first polished using 1200- and 4000-grid waterproof silicon carbide paper to reduce end frictions during the low and high strain rate deformation, and then greased for low- and room temperature tests.

Compression tests at strain rates of 0.001/s and 0.1/s are preformed using an Instron hydraulic testing machine at temperatures ranging from 77 K to 600 K, with the maximum achieved true strain exceeding about 80%. Temperature elevation is achieved by using a high-intensity quartz-lamp in a radiant-heating furnace. The temperature is measured using a thermocouple arrangement. Constant temperatures can be maintained within ±2 °C. The deformation of the specimens is measured by LVDT mounted in the testing machine. The measuring facility is calibrated with standard

* Corresponding author.
E-mail address: weiguo@nwpu.edu.cn (W.G. Guo).

0997-7538/$ – see front matter © 2010 Elsevier Masson SAS. All rights reserved.
doi:10.1016/j.euromechsol.2010.09.001

Table 1
Major alloy content of 3003 Al–Mn alloy (wt %).

Mn	Fe	Si	Cu	Zn	Other	Al
1.0–1.5	0.7	0.6	0.05–0.20	0.1	<0.15	Remainder

extensometer before the tests. The low temperature of 77 K is achieved by immersing the specimen and testing fixture in a bath of liquid nitrogen. Typical true stress–strain curves of 3003 Al–Mn alloy at a constant strain rate of 0.001/s and with different temperatures are shown in Fig. 1.

Dynamic tests at a strain rate of 3200/s with different temperatures are performed using an enhanced split Hopkinson pressure bar (enhanced SHPB) (Nemat-Nasser and Isaacs, 1997). The configuration of the enhanced SHPB for compression testing is shown in Fig. 2. It consists of two identical elastic pressure bars of maraging 300 steel with the yield stress exceeding 2000 MPa. The dimensions of the bars are 12.7 mm in diameter and 1.2 m in length. For such high temperature dynamic tests, it is necessary to heat the sample to the desired temperature and, in the mean while, keep the incident and transmission bars at a suitable low temperature. In order to do this, the bars are kept outside the range of the heating wire in the furnace, and the specimen held by the thermocouple is positioned at the center of the furnace by a Cu sleeve. Once the specimen is heated to the target temperature, the bars are then brought into contact with the specimen right before the stress pulse reaches the end of the incident bar. This task is accomplished by the employment of a transmitter bar mover, which can be driven by synchro pneumatic pressure from an actuation assembly in the same time as the strike bar is fired. The temperature of specimen can be measured by thermocouple that is holding the specimen inside the furnace. The true stress–strain curves at a strain rate of 3200/s with different temperatures are shown in Fig. 3.

In order to ensure the validity of experimental data, all stress–strain curves are obtained by testing at least three samples. If the curves for three samples have remarkable scatter, more samples are needed to repeat the test until the experimental data are observed to possess good repeatability or less scatter. It turns out that good repeatability and consistency of the testing results is obtained, probably resulting from shear-glide domination during the plastic flow for metals.

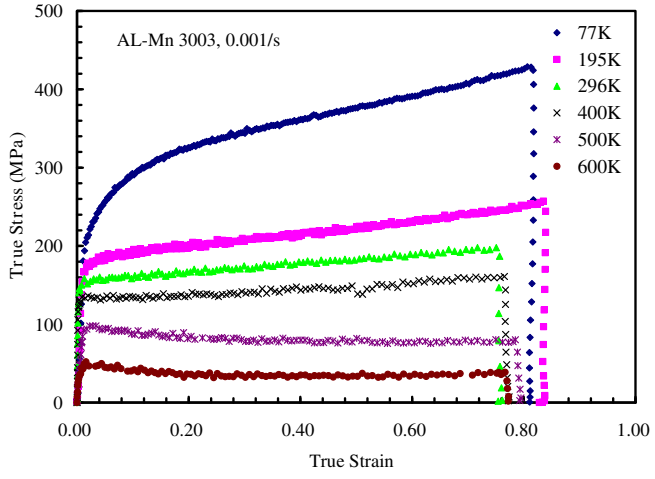

Fig. 1. True stress–true strain curves at indicted temperatures and a strain rate of 0.001/s.

3. Experimental results

3.1. Temperature effect on the flow stress

It has been noticed from Figs. 1 and 3 that the plastic flow stress of 3003 Al–Mn alloy remarkably decreases as the temperature increases from 77 K to 820 K, meaning that the flow stress is very sensitive to temperature change. For experimental data at strain rate of 0.001/s and temperature of 77 K shown in Fig. 1, the plastic strain is observed to be greater than 80%. It has been observed in Fig. 1 that the strain hardening rate slightly decreases as the strain increases for temperature above 500 K at the strain rate of 0.001/s. Such decrease is possibly caused by stress relaxation due to creep deformation under high temperatures and low strain rate. It is noticed as well in Fig. 3 that the strain hardening quickly decreases at strain rate of 3200/s and temperature of 77 K. This phenomenon is possibly due to the deformation localization or occurrence of shearband inside the sample for low temperature tests. The strained samples do not present visible crack or break in appearance. Uniform deformation has been observed through all tested samples, indicating excellent plastic formability and ductility even at low temperatures.

3.2. Strain rate effect on the flow stress

Fig. 4 shows the stress–strain curves of 3003 Al–Mn alloy at temperature of 296 K with various applied strain rates. It is noticed that the flow stress of 3003 Al–Mn alloy is strongly depending on the applied strain rate, especially when the strain rate is above the order of 10^3/s (see the result of 9.500/s for instance). The dependence of the flow stress on temperature at a fixed strain of 0.1 is presented in Fig. 5 for different applied strain rates. It can be seen that the strain rate effect increases with decreasing temperature for dynamic tests, and the greatest strain rate effect is observed around the temperature of 77 K. In Fig. 6, true stresses as a function of strain rates are plotted for a fixed strain of 0.2 and initial temperature of 296 K. It is noticed that the flow stress increases nonlinearly with increasing strain rate. The nonlinearity is more notable with strain rates higher than the order of 10^3/s. Such strain rate effect is usually attributed to the electron- and phonon-drag effect on the mobile dislocations (Follansbee and Weertman, 1982; Zerilli and Armstrong, 1992; Chiem, 1992; Regazzoni et al., 1987).

3.3. The 3rd dynamic strain aging phenomenon

Based on the observation of Figs. 1 and 3, it has been known that the plastic flow stress of 3003 Al–Mn alloy is strongly depending on temperature. To further reveal the temperature effect on flow stresses, the data in Figs. 1 and 3 are re-organized and plotted in Figs. 7 and 8. In these figures, the flow stresses are plotted as functions of temperature for given strains and certain strain rate. During the temperature increase from 77 K, the temperature of liquid nitrogen, to about 600 K, the flow stress first decreases rapidly, and then the decrease starts to slow down when the temperature is above 300 K. Actually for temperature above 300 K, there exist occasions that the temperature has very little effect on the flow stresses. Such unusual phenomenon is considered the 3rd dynamic strain aging (Guo, 2007; Guo and Nemat-Nasser, 2006; Nemat-Nasser et al., 1999).

Frequently dynamic strain aging (DSA), often called Portevin–Lechatelier effect, is defined as recurrent pinning (discontinuous or repeated yielding) of dislocations during plastic deformation (Kubin et al., 1992; Klose et al., 2003). The DSA is attributed to the additional resistance to dislocation motion produced by the mobility of solute atoms that can diffuse to dislocations above a certain temperature (Hong et al., 2005; Beukel and Kocks, 1982) while the

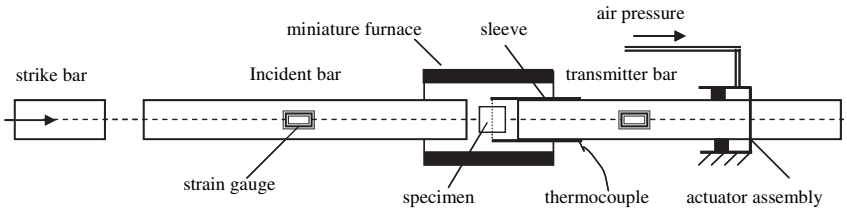

Fig. 2. Configuration of the enhanced split Hopkinson pressure bar.

dislocations are "waiting" at their short-range barriers. During this waiting period, a Cottrell atmosphere and/or a core atmosphere can form at dislocations, depending on the temperature and strain rate (Nakada and Keh, 1970). That is, the solute atoms are able to diffuse in the specimen at a rate faster than the speed of the dislocations so as to catch and lock them. The vacancies needed for the solute atoms to diffuse is produced by a plastic deformation, so, to start recurrent yields phenomena, the critical plastic strain for the onset of serration is needed (Peng et al., 2006).

For DSA in aluminum alloys, Peng et al. (2006) have confirmed the DSA existence and presented characteristics of the serrated flow in aluminum alloy and Al–Mg alloys, and obtained the onset plastic strain for serrations. Using thermal fields, Louche et al. (2005) have given the spatio-temporal distribution of PLC bands in Al–4 wt.% Mg alloy sheet. Klose et al. (2004) have presented an analysis of stress drops for constant strain rate tensile tests on Al–(1.5–4.5) wt.% Mg in terms of their dependencies on temperature and strain rate for type B deformation bands. Based on the assumption of dislocation pile-ups exerting local stress concentrations necessary to initiate PLC band propagation, a simple model is confirmed and extended here by applying it to the PLC stress serrations in Al–Mg.

For the present investigation on 3003 Al–Mn alloy, based on the experimental observations, we suggest the existence of 3rd *dynamic strain aging*, which is a little different to PLC (refer to Guo, 2007; Guo and Nemat-Nasser, 2006 for details). The occurring temperature region is from 300 K to 500 K for a strain rate of 0.001/s, and from 300 K to 600 K for a strain rate of 3200/s.

3.4. Temperature and strain rate history effect on the flow stress

In this section, interrupted tests are performed to investigate the microstructural evolution in 3003 Al–Mn alloy, whose mechanical properties can be affected by strain rate and temperature. Firstly the strain rate history effect on the flow stress is examined by compression tests with strain rate changing from 0.001/s to 0.1/s. As shown in Fig. 9, the stress–strain curves at strain rate of 0.001/s and 0.1/s are obtained for sample 1 and sample 2, respectively, at initial temperature of 195 K. Sample 3 is initially loaded to a true strain of about 6% at a strain rate of 0.001/s and at temperature of 195 K. After unloading, sample 3 is reloaded at a different strain rate of 0.1/s for the same temperature. It is noticed that this interrupted reloading stress–strain curve basically follows the curve that has been obtained for continuous loading at strain rate of 0.1/s. Only slight difference is observed for these two procedures. In the mean while, we noticed that, Khaleel et al. (1997) have shown that the strain rate history often affects the subsequent work hardening in metals, but it does not affect the true strain at failure; Klepaczko (1975) have demonstrated that the strain rate history effect plays a very important role in the plastic behavior of polycrystalline f.c.c. metals. These observations are attributed to differences in the effective dislocation multiplication rates for different strain rates. In this work, however, the interrupting tests show that pre-straining of 3003 Al–Mn alloy at different strain rates will not cause significant change of microstructures to affect the subsequent mechanical response.

Fig. 10 shows the temperature history effect on the flow stress of 3003 Al–Mn alloy. At the applied strain rate of 0.001/s, sample 4 and sample 5 are loaded to a true strain of 40% at temperature of 296 K and 77 K, respectively. Under the same strain rate, sample 6 is initially loaded to a true strain of around 7% at the temperature of 296 K and subsequently unloaded. After that, sample 6 is cooled to 77 K, and then reloaded at the same strain rate. As it shows in Fig. 10, the flow stress of sample 6 deviates substantially from that of sample 5. Therefore it shows that the temperature history during the deformation of 3003 Al–Mn alloy does significantly affect the

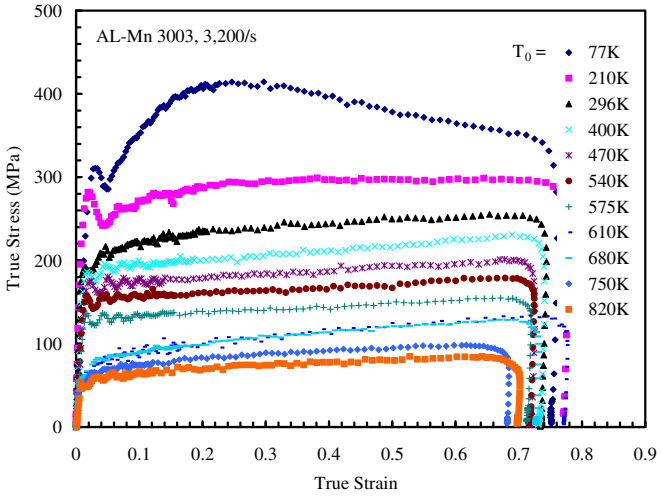

Fig. 3. True stress–true strain curves at indicted initial temperatures and a strain rate of 3200/s.

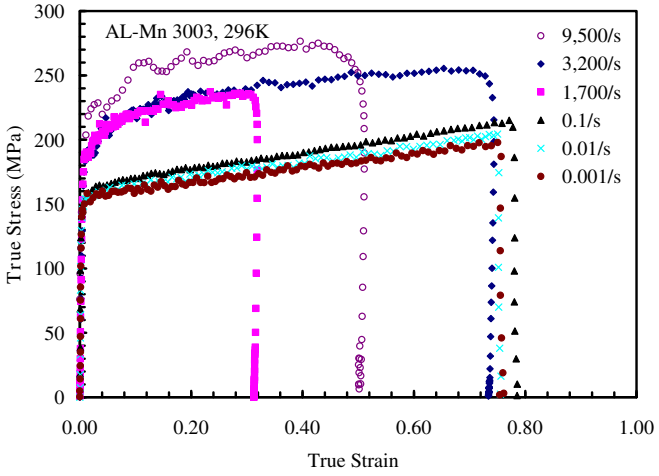

Fig. 4. Effect of strain rates on flow stress at initial temperature 296 K.

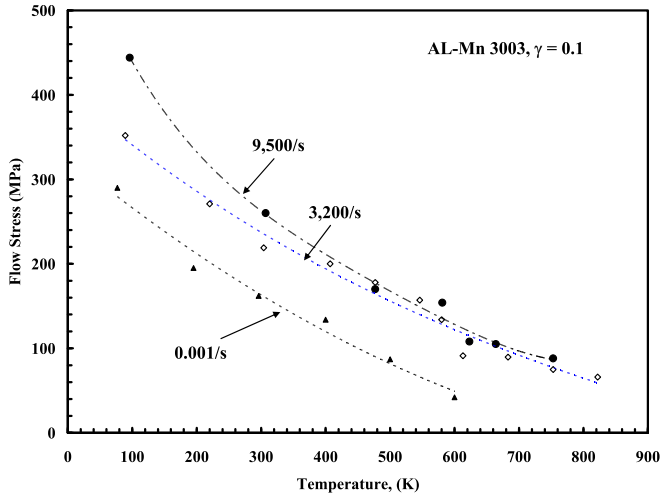

Fig. 5. Effect of strain rates on flow stress at a fixed true strain of 0.1.

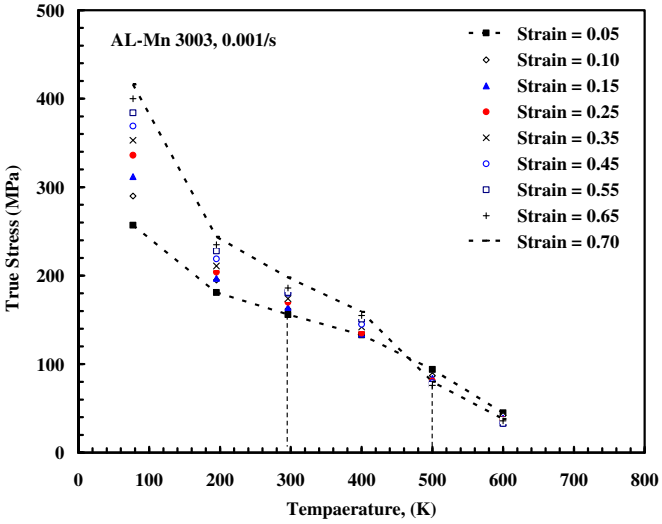

Fig. 7. Flow stress as a function of temperature for indicated strains and 0.001/s strain rate.

subsequent stress–strain response. It further implies that the pre-applied temperature will cause evolution of microstructures within 3003 Al–Mn alloys.

In summary of the above mentioned experimental results, it is concluded that, (1) the plastic flow stress of 3003 Al–Mn alloy strongly depends on applied temperatures and strain rates; (2) possibly due to viscous-drag effect on the flow, the flow stress of 3003 Al–Mn alloy rapidly increases with increasing strain rate especially when the strain rate is over the order of 10^3/s; (3) the 3rd *dynamic strain aging* occurs at the temperature of around 300 K with the applied strain rate of 0.001/s, whereas it occurs between 300 K and 600 K for applied strain rate of 3200/s; (4) pre-applied temperature will cause remarkable microstructural evolution within 3003 Al–Mn alloy.

4. Constitutive modeling

4.1. Evaluation of plastic work–heat conversion factor

Plastic deformation generates heat, which is either dissipated to the surroundings or used to increase the temperature of the material. When the rate of heat generation is greater than heat loss, the temperature rises. This generally happens for the case of high strain rate loading. For materials whose flow stress is temperature-dependent, a continuous rise in temperature during deformation can result in simultaneous lowering of the flow stress. The temperature rise of a 3003 Al–Mn alloy sample during adiabatic testing procedure can be calculated by

$$\Delta T = \int_0^{\gamma} \frac{\beta}{\rho' C_V} \tau \mathrm{d}\gamma, \tag{1.1}$$

where ρ' is the mass density (2.73 g/cc), C_V the temperature-dependent heat capacity (0.892 J/g K at room temperature), γ the plastic strain, and τ the flow stress in MPa. The Taylor–Quinney coefficient β, which indicates the fraction of plastic work that is converted into heat, has been shown by Hodowany et al. (2000) to approach 1.0 for aluminum alloys for strains greater than 15%. Data reported by Kapoor and Nemat-Nasser (1998) for several metals suggest that, for large strains (e.g., $\gamma > 20\%$), β is essentially 1. This has also been verified to be the case for several other polycrystalline

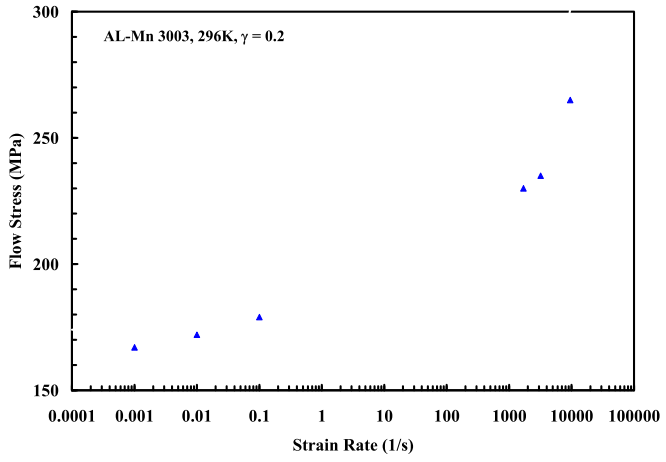

Fig. 6. True stress as a function of strain rates for an initial temperature 296 K and at a fixed true strain of 0.2.

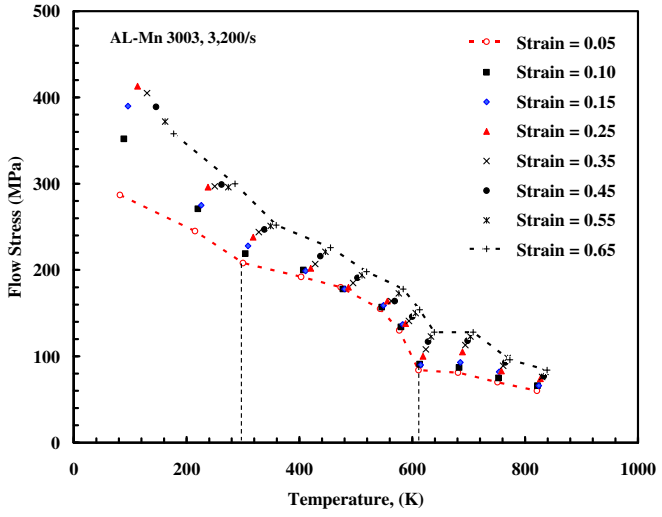

Fig. 8. Flow stress as a function of temperature for indicated strains and 3200/s strain rate.

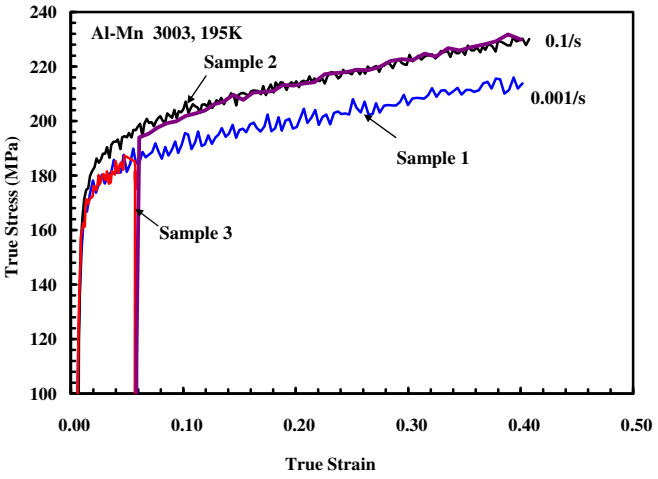

Fig. 9. Effect of strain rate jump from 0.001/s to 0.1/s on flow stress.

metals, see Nemat-Nasser et al. (1999, 2001). In the present study, we take $\beta = 1.0$.

To examine the applicability of the proposed value of β for 3003 Al–Mn alloy in this study, an indirect experiment is performed knowing that the area under the true stress–true strain curve gives the plastic work per unit volume in uniaxial deformation. Fig. 11 shows the results of uniaxial compression tests, where three samples (designated as 1, 2, and 3, respectively) are loaded at the same strain rate of 3200/s. The basic idea for this indirect experiment lies in the followings: the mechanical behavior of sample 1 is taken as a reference for adiabatic loading procedure, during which the temperature rise takes effect on the flow stress; starting from an intermediate point of the procedure, the same loading test is performed on sample 2 but with artificially induced temperature that is calculated by Eq. (1.1) with the assumption of $\beta = 1.0$, such that the applicability of the calculation can be checked by comparing the measured responses between sample 1 and sample 2; a third sample is taken for the same test on sample 2 but without artificially induced temperature such that the temperature effect of flow stress can be observed by comparing the responses between sample 1 and sample 3.

Based on the above mentioned steps, sample 1 is loaded to a true strain of around 76% at an initial room temperature of 21.6 °C. The corresponding true stress–true strain curve is displayed by the dot curve in Fig. 11. This is essentially an adiabatic procedure, where

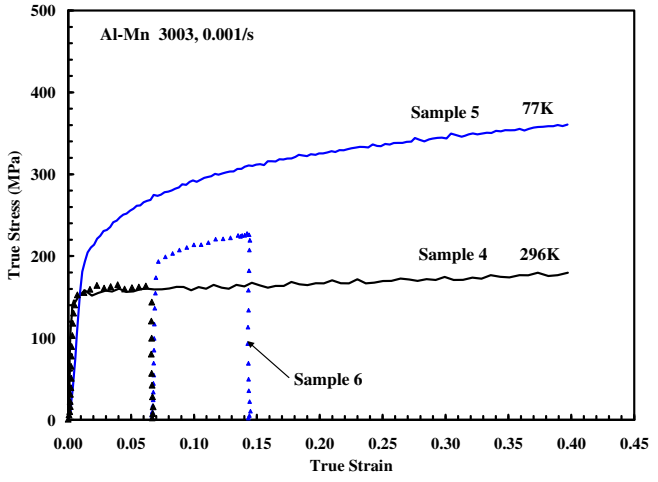

Fig. 10. Effect of temperature jump from 296 K to 77 K on flow stress.

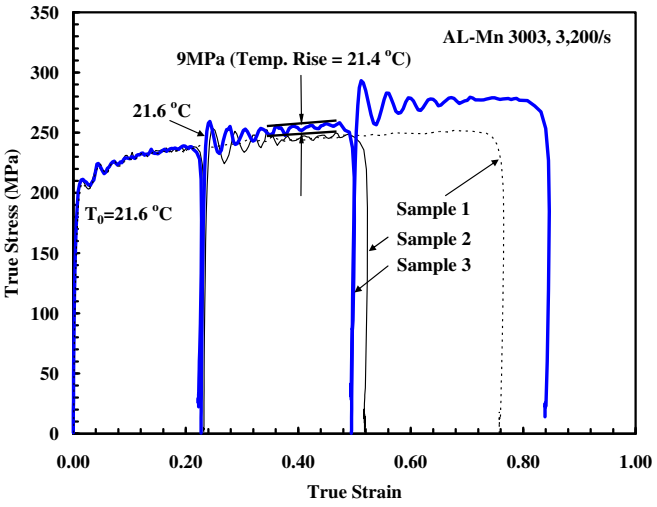

Fig. 11. Verification of heat conversion.

temperature rise will affect the flow stress. The corresponding result of sample 2 during the compression test is displayed by thin solid curve shown in Fig. 11. Sample 2 is first loaded to a true strain of 24%, starting from room temperature of 21.6 °C at the same strain rate. The response for this portion of the procedure is identical to that of sample 1, showing the reproducibility of the experiment. The temperature rise at true strain of 24% is calculated to be 21.4 °C by Eq. (1.1) with the assumption of $\beta = 1.0$. After being unloaded and cooled to room temperature, sample 2 is heated to 43 °C that corresponds to the initial temperature of 21.6 °C plus the calculated temperature rise of 21.4 °C. Sample 2 is then reloaded at the same strain rate, producing the second part of the curve as shown in Fig. 11. It is noticed that this portion of the curve coincides with that of sample 1, therefore verifying the applicability of the calculation for temperature rise. To see the effect on flow stress due to temperature rise, sample 3 experiences the same loading and unloading procedure as sample 2 with an achieved strain of 24%. After being cooled to room temperature, however, sample 3 is reloaded without any induced temperature. This approach can construct an isothermal flow stress at a high strain rate (Nemat-Nasser and Isaacs, 1997). The response of sample 3 during the testing procedure is displayed by thick solid curve in Fig. 11. It is clear that there is difference on flow stress between the adiabatic and isothermal procedures due to thermal softening of the material. The difference is roughly measured to be 9 MPa for the strain increment of 24%. It can be seen from Fig. 11 that another unloading and isothermal reloading is conducted on sample 3 at the strain of around 49%. The thermal softening is certainly more remarkable. Based on the observations, two important conclusions can be drawn: 1) after the sample being unloaded and cooled to the initial temperature, there will be no noticeable change in flow stress upon reloading if the temperature can be recovered to its original state; and 2) during the calculation of temperature rise in the present work, essentially the entire plastic work can be considered to convert to heat with a negligibly small amount being stored in the sample as the elastic energy of the dislocations and other defects, or lost through sample boundaries.

4.2. Physically-based constitutive model

Presently, there exist integrated constitutive equations relating plastic flow stress with strain, strain rate, and temperature (Sung et al., in press). Unlike phenomenological models, which are determined directly from experimental data, physical models are especially useful in specific applications where the calculated

variables can be related to experimental observations (such as dislocation density) (Durrenberger et al., 2007). Bases on the separation of the constant-structure part of the strain rate sensitivity from the structure evolution part, Follansbee and Kocks (1988) have proposed a physical model, the MTS (Mechanical-Threshold-Strength) model. Nes and Marthinsen (2002) recently have developed an alternative work hardening model, the MPM model (Nes et al., 2001; Marthinsen and Nes, 1997). With the help of the illumination of the MTS model, in terms of f.c.c. metals' plastic deformation and the structural evolution characteristics, Nemat-Nasser and Li (1998) have developed a model for f.c.c. metals. It is known that 3003 Al–Mn alloy mainly presents f.c.c. structural characteristics. Therefore, based on the concept of dislocation kinetics and paralleled with the systematic experimental investigation, a physically-based model for 3003 Al–Mn alloy is introduced with the aid of framework suggested by Nemat-Nasser and Li (1998). The dynamic strain aging effects are not included in this model.

$$\tau = 72\left\{1-\left[-3.2\times10^{-5}T\left(\ln\frac{\dot\gamma}{2\times10^{10}}+\ln f(\gamma,T)\right)\right]^{1/q}\right\}^{1/p}\times f(\gamma,T)+64\gamma^{0.4},$$
$$T = T_0+0.41\int_0^\gamma \tau d\gamma,\quad f(\gamma,T) = 1+6\left[1-\left(\frac{T}{916}\right)^2\right]\gamma^{0.05}. \tag{1.6}$$

For 3003 Al–Mn alloy, the flow stress τ is considered to fall into two parts: τ^*, which is essentially due to the short-range thermal-activated effect, and an athermal component, τ_a, which is mainly due to the long-range effects. The total flow stress can be expressed as $\tau=\tau_a+\tau^*$. The athermal stress component τ_a is independent to the strain rate, $\dot\gamma$, and can be assumed to take the form of $\tau_a\approx a_0+a_1\gamma^n$, where a_0, a_1, and n are free parameters that should be determined experimentally. The thermally-activated component τ^*, in general, is a function of temperature T, strain rate $\dot\gamma$, and the internal evolution variables of the material. To obtain the relation among $\dot\gamma$, T and τ^*, an association between the activation free energy ΔG and τ^* needs to be obtained. Kocks et al. (1975) suggested an empirical relation between ΔG and τ^*, representing a typical barrier encountered by a dislocation. The relation can be written as

$$\Delta G = G_0\left[1-\left(\frac{\tau^*}{\hat\tau}\right)^p\right]^q, \tag{1.2}$$

where $0<p\le1$ and $0\le q\le1$. Here $\hat\tau$ is the shear stress above which the barrier is crossed by a dislocation without any assistance from thermal activation, and G_0 is the free energy required to overcome the barrier when the applied stress τ^* is zero. It is also known that $\dot\gamma$ can be related to ΔG by

$$\dot\gamma = \dot\gamma_0\exp\left(-\frac{\Delta G}{kT}\right), \tag{1.3}$$

where $\dot\gamma_0$ is a pre-exponential term, and k is the Boltzmann constant. Eqs. (1.2) and (1.3) together yield the following expression for τ^*:

$$\tau^* = \left\{\hat\tau\left[1-\left(\frac{kT}{G_0}\ln\frac{\dot\gamma}{\dot\gamma_r}\right)^{1/q}\right]^{1/p}\right. . \tag{1.4}$$

It has been concluded from experimental results in Section 3.4 that the microstructure in 3003 Al–Mn alloy tends to evolve substantially with preloading temperature and strain (γ, T), but will not evolve remarkably with the preloading strain rate $\dot\gamma$. Therefore to account for the microstructural evolution in the thermally-activated part of flow stress, by referring to the work of Nemat-Nasser and Li (1998), the dimensionless term $f(\gamma,T)$ is introduced to $\hat\tau$ and the reference strain rate $\dot\gamma_r$ in Eq. (1.4) to describe the amount of microstructural evolution. The thermal-activated part of the flow stress, τ^*, then becomes

$$\tau^* = \tau^0\left\{1-\left[-\frac{kT}{G_0}\left(\ln\frac{\dot\gamma}{\dot\gamma_0}+\ln f(\gamma,T)\right)\right]^{1/q}\right\}^{1/p}\times f(\gamma,T), \tag{1.5}$$
$$\text{where,}\quad f(\gamma,T) = 1+a\left[1-\left(\frac{T}{T_m}\right)^2\right]\gamma^{1/2}.$$

In Eq. (1.5), T_m is melting temperature, and $\tau^0$and a are material constants. The parameters in Eq. (1.5) are obtained through calculations based on experimental results and substitutions of the values of physical constants as described in the work of Nemat-Nasser and Li (1998). The final constitutive equations for 3003 Al–Mn are then given as

Figs. 12–15 have shown the comparison between experimental results and the model predictions for strain rates ranging from 0.001/s to 9500/s at different initial temperatures. A good match has been observed between the experimental observations and theoretical results.

5. Discussion and conclusions

5.1. Analysis on the experimental results

The initial strain hardening rate of fcc metals during plastic flow is often observed to dramatically increase with strain rates (Follansbee and Kocks, 1988). But according to the testing results

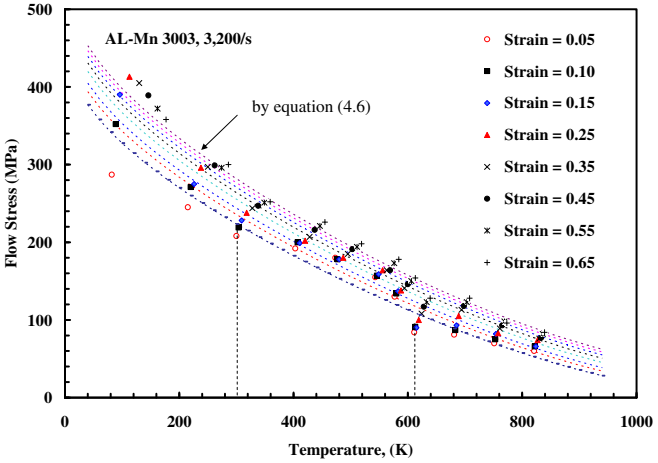

Fig. 12. Flow stress as a function of temperature with given strains at strain rate of 3200/s. The experimental results are depicted by discrete data with the given strains shown in the legend. The corresponding calculated results by Eq. (1.6) at given strains are plotted as continuous small dots with the order of, from top to bottom, strain = 0.65 to strain = 0.05.

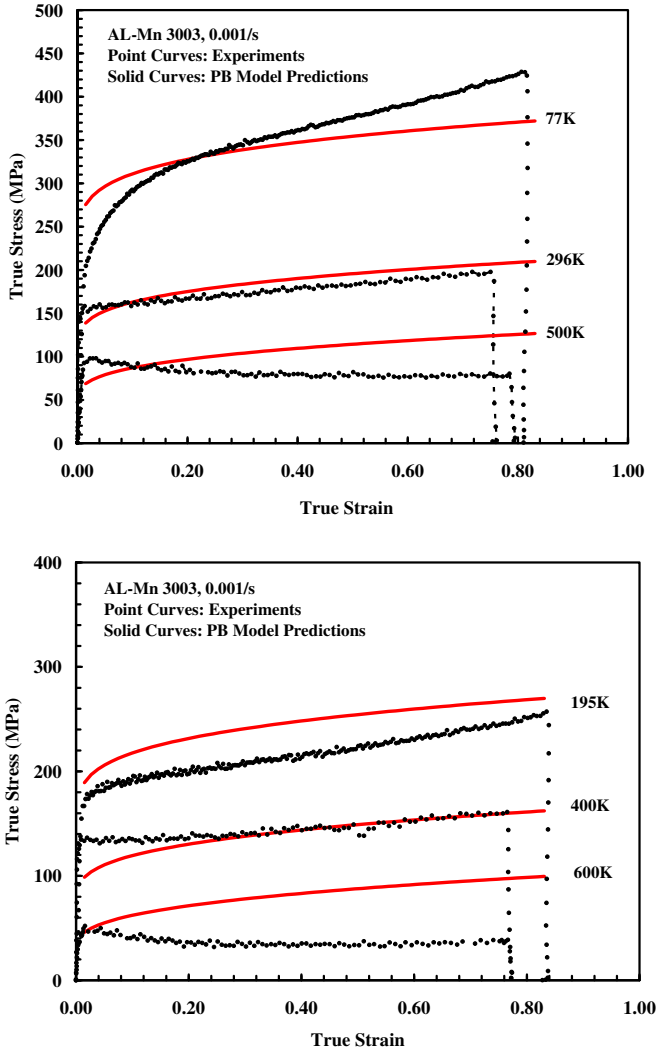

Fig. 13. Comparison of model predictions with experimental results at a strain rate of 0.001/s.

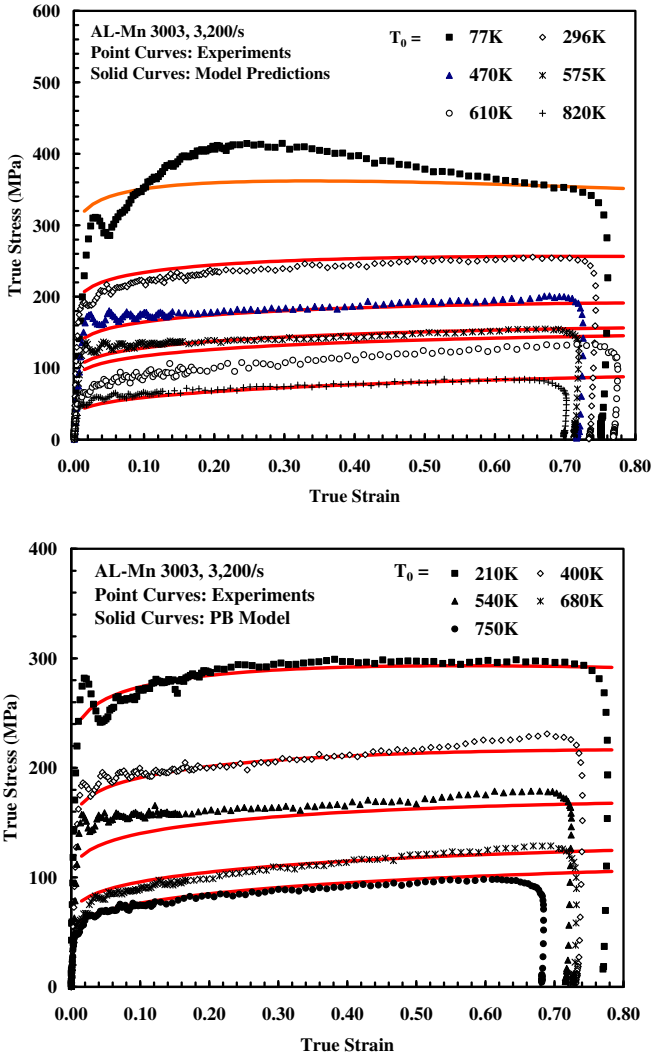

Fig. 14. Comparison of model predictions with experimental results at a strain rate of 3200/s.

shown in Figs. 1 and 3, we have noticed that the strain hardening rate of the 3003 Al–Mn alloy during plastic flow only has a slow increase with the increasing strain, and it even decreases when the temperature is over 500 K at the strain rate of 0.001/s. Such decrease is possibly caused by stress relaxation due to creep deformation under high temperatures and low strain rate. Since more alloy elements are added into the aluminum, the 3003 Al–Mn alloy seems to present bcc metal's characteristics during plastic flow (Nemat-Nasser and Guo, 2003). By observing the results of strain rate jumping test shown in Fig. 9, it has been noticed that the strain rate history has little effect on plastic flow for 3003 Al–Mn alloy. This finding further implies that the microstructure or dislocation density is not significantly affected by strain rate history. It is observed that temperatures and strains have strong effects on plastic flow stress of the 3003 Al–Mn alloy.

The dynamic strain aging, so-called Portevin–Lechatelier effect, is a common phenomenon in most metals, especially in fcc metals. As it has been discussed in Section 3.3, during the temperature increase from 77 to around 600 K, the flow stress first decreases rapidly, and then the decrease starts to slow down with temperatures above 300 K. For temperatures above 300 K, there exist occasions that the temperature has very little effect on the flow stresses. The temperature range that has little effect on flow stress is 300–500 K for a strain rate of 0.001/s and 300–600 K for a strain rate of 3200/s. Based on the experimental observations in Section 3.3, it is believed that the DSA occurs only in a certain combined range of temperature and strain rate. The existence of the 3rd dynamic strain aging phenomena needs some pre-deformation and thus abundance vacancies are produced. These vacancies avail interstitial diffusion around the dislocation. In post continuous plastic deformation, the interstitial atoms atmosphere around the dislocation continually drag and increase gliding resistance to the dislocation motion, this lead to the 3rd dynamic strain aging phenomena. Therefore the mechanism of third DSA is considered as the rapid/continuous formation of the solute atmospheres at the mobile dislocation core by the pipe diffusion along vast collective forest dislocations to result in a continuous rise curve of flow stress (Guo, 2007).

5.2. Analysis on the modeling results

Figs. 13–15 have shown the comparison between experimental results and the model predictions for strain rates ranging from 0.001/s to 9500/s at different initial temperatures. A good match has been observed between the experimental observations and theoretical results.

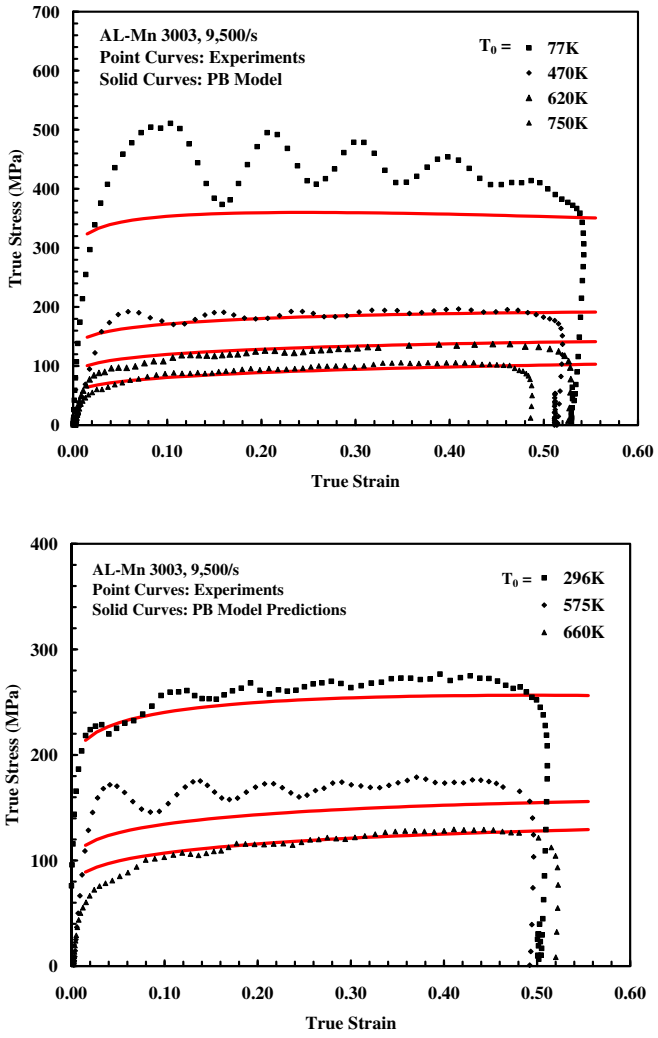

Fig. 15. Comparison of model predictions with experimental results at a strain rate of 9500/s.

As it has been pointed out previously, this model does not include the dynamic strain aging effects, which occur in the temperature range from 300 K to 600 K. Therefore the experimental results and model predictions are not in a perfect agreement within such temperature range. This can be observed in the comparisons shown in Figs. 12 and 13 for temperatures of 500 K and 600 K.

For the comparisons shown in Fig. 15 at strain rate of 9500/s with initial temperature of 77 K, the discrepancy between experimental results and model predictions is possibly due to the change of plastic flow/deforming mechanism, *e.g.,* adiabatic shear effect in low temperatures and high strain rates. The large oscillation for the testing data in Fig. 15 is due to dissipated effect of the stress wave propagation. It is actually a ringing phenomenon from the Hopkinson bar test, and is not modeled in the theoretical study.

In summary of this work, the uniaxial deformation behavior of 3003 Al–Mn alloy over a wide range of strain rates and temperatures has been systematically studied. The following findings have been concluded: 1) the 3003 Al–Mn alloy displays remarkable ductility and plasticity at low temperatures and high strain rates; (2) the yield stress and the plastic flow stress of 3003 Al–Mn alloy strongly depends on temperatures and strain rates; (3) the temperature history during deformation strongly affects the microstructure evolution of this material. Finally, paralleled with the systematic experimental investigations, a physically-based model is developed for the deformation behavior of this material. The model predictions are compared with the experimental results, and a good agreement has been observed.

Acknowledgement

The present work was supported by the National Natural Science Fund of China (10872169), and the Research Fund of State Key Laboratory of Explosion Science and Technology (KFJJ08-11). Authors also thank the support from Major State Basic Research Development Program (973 program) (No. 613116) and the support from Beijing Municipal Education Commission Project (20080739027).

References

Beukel, A.V.D., Kocks, U.F., 1982. The strain dependence of static and dynamic strain-aging. Acta Metall. 30, 1027–1034.
Barlat, F., Glazov, M.V., Brem, J.C., et al., 2002. A simple model for dislocation behavior, strain and strain rate hardening evolution in deforming aluminum alloys. Int. J. Plasticity 18, 919–939.
Chiem, C.Y., 1992. Material deformation at high strain rates. In: Meyers, M., Murr, L., Staudhammer, K. (Eds.), Shock-wave and High-Strain-Rate Phenomena in Materials. Marcel Dekker, Inc, pp. 69–85.
Durrenberger, L., Klepaczko, J.R., Rusinek, A., 2007. Constitutive modeling of metals based on the evolution of the strain-hardening rate. J. Eng. Mater. Technol. 129, 550–557.
Follansbee, P.S., Kocks, U.F., 1988. A constitutive description of the deformation of copper based on the use of the Mechanical Threshold Stress as an internal state variable. Acta Metall. 36, 81–93.
Fujii, T., Watanabe, C., Nomura, Y., et al., 2002. Microstructural evolution during low cycle fatigue of a 3003 aluminum alloy. Mater. Sci. Eng. A 319–321, 592–596.
Follansbee, P.S., Weertman, J., 1982. On the question of flow stress at high strain rates controlled by dislocation viscous flow. Mech. Mater. 1, 345–350.
Guo, W.G., 2007. Dynamics strain aging during the plastic flow of metals. Key Eng. Mater. 340–341, 823–828.
Guo, W.G., Nemat-Nasser, S., 2006. Flow stress of Nitronic-50 stainless steel over a wide range of strain rates and temperatures. Mech. Mater. 38, 1090–1103.
Hong, S.G., LeeKeum, O., LeeSoonBok, 2005. Dynamic strain aging effect on the fatigue resistance of type 316L stainless steel. Int. J. Fatigue 27, 1420–1424.
Hodowany, J., Ravichandran, G., Rosakis, A.J., Rosakis, P., 2000. Partition of plastic work into heat and stored energy in metals. Exp. Mech. 40, 113–123.
Kapoor, R., Nemat-Nasser, S., 1998. Determination of temperature rise during high strain rate deformation. Mech. Mater. 27, 1–12.
Kocks, U.F., Argon, A.S., Ashby, M.F., 1975. In: Chalmers, B., Christian, J.W., Massalski, T.B. (Eds.), Thermodynamics and Kinetics of Slip. Progress in Materials Science, vol. 19. Pergamon Press, Oxford, pp. 120–129.
Khaleel, M.A., Smith, M.T., Pitman, S.G., 1997. The defect of strain rate history on the ductility in superplastic AA-5083. Scripta Materialia 37 (2), 1909–1915.
Kubin, L.P., Estrin, Y., Perrier, C., 1992. On static strain ageing. Acta Metall. 40, 1037–1044.
Klose, F.B., Ziegenbein, A., Weidenmuller, J., Neuhäuser, H., Hähner, P., 2003. Portevin–LeChatelier effect in strain and stress controlled tensile tests. Comput. Mater. Sci. 26, 80–86.
Klose, F.B., Ziegenbein, A., et al., 2004. Analysis of Portevin-Le Chatelier serrations of type Bin Al–Mg. Mater. Sci. Eng. A369, 76–81.
Klepaczko, J., 1975. Thermally activated flow and strain rate history effects for some polycrystalline f.c.c. metals. Mater. Sci. Eng. 18, 121–135.
Luan, B., Le, T., Nagata, J., 2004. An investigation on the coating of 3003 aluminum alloy. Surf. Coat. Technol. 186 (3), 431–443.
Liu, W.C., Zhai, T.J., Morris, G., 2004. Texture evolution of continuous cast and direct chill cast AA 3003 aluminum alloys during cold rolling. Scripta Materialia 51, 83–88.
Louche, H., Vacher, P., Arrieux, R., 2005. Thermal observations associated with the Portevin–Le Ch-atelier effect in an Al–Mg alloy. Mater. Sci. Eng. A 404, 188–196.
Marthinsen, K., Nes, E., 1997. A general model for metal plasticity. Mater. Sci. Eng. A234-236, 1095–1098.
Nemat-Nasser, S., Guo, W.G., Cheng, J.Y., 1999. Mechanical properties and deformation mechanisms of a commercially pure titanium. Acta Mater. 47, 3705–3721.
Nemat-Nasser, S., Guo, W.G., Kihl, D.P., 2001. Thermomechanical response of AL-6XN stainless steel over a wide range of strain rates and temperatures. J. Mech. Phys. Solids 49, 1823–1846.
Nemat-Nasser, S., Li, Y.L., 1998. Flow stress of fcc polycrystals with application to OFHC Cu. Acta Mater. 46, 565–577.

Nemat-Nasser, S., Isaacs, J.B., 1997. Direct measurement of isothermal flow stress of metals at elevated temperatures and high strain rates with application to Ta and Ta–W alloys. Acta Mater. 45 (3), 907–919.
Nemat-Nasser, S., Guo, W.G., 2003. Thermomechanical response of DH-36 structural steel over a wide range of strain rates and temperatures. Mech. Mater. 35, 1023–1047.
Nakada, Y., Keh, A.S., 1970. Serrated flow in Ni–C alloys. Acta Metall. 18, 437–443.
Nes, E., Marthinsen, K., Ronning, B., 2001. Modelling the evolution in microstructure and properties during processing of aluminium alloys. J. Mater. Process. Technol. 117, 333–340.
Nes, E., Marthinsen, K., 2002. Modeling the evolution in microstructure and properties during plastic deformation of f.c.c.-metals and alloys – an approach towards a unified model. Mater. Sci. Eng. A322, 176–193.
Peng, K., Chen, W., Qian, K., 2006. Study on dynamic strain aging phenomenon of 3004 aluminum alloy. Mater. Sci. Eng. A415, 53–58.
Regazzoni, G., Kocks, U.F., Follansbee, P.S., 1987. Dislocation kinetics at high strain rates. Acta Metall. 35, 2865–2875.
Sung, J.H., Kim, J.H., Wagoner, R.H., 2010. A plastic constitutive equation incorporating strain, strain-rate, and temperature. Int. J. Plasticity, doi:10.1016/j.ijplas.2010.02.005.
Woodcraft, A.L., 2005. Predicting the thermal conductivity of Aluminium alloys in the cryogenic to room temperature range. Cryogenics 45, 421–431.
Yeh, C.L., Chen, Y.F., Wen, C.Y., et al., 2003. Measurement of thermal contact resistance of aluminum honeycombs. Exp. Thermal Fluid Sci. 27, 271–281.
Zerilli, F.J., Armstrong, R.W., 1992. The effect of dislocation drag on the stress-strain behavior of f.c.c. metals. Acta Metall. Matter. 40, 1803–1808.